



ARTICLE

Fluid-Related Performances and Compressive Strength of Clinker-Free Cementitious Backfill Material Based on Phosphate Tailings

Jin Yang^{1,2}, Senye Liu¹, Xingyang He^{1,2,*}, Ying Su^{1,2}, Jingyi Zeng² and Bohumír Strnadel^{1,3}

¹School of Civil Engineering, Architecture and Environment, Hubei University of Technology, Wuhan, 430068, China

²Building Waterproof Engineering and Technology Research Center of Hubei Province, Hubei University of Technology, Wuhan, 430068, China

³Center of Advanced Innovation Technologies, VŠB-Technical University of Ostrava, 708 33 Ostrava-Poruba, Czech Republic

*Corresponding Author: Xingyang He. Email: 20041008@hbut.edu.cn

Received: 04 February 2024 Accepted: 06 May 2024 Published: 23 August 2024

ABSTRACT

Phosphate tailings are usually used as backfill material in order to recycle tailings resources. This study considers the effect of the mix proportions of clinker-free binders on the fluidity, compressive strength and other key performances of cementitious backfill materials based on phosphate tailings. In particular, three solid wastes, phosphogypsum (PG), semi-aqueous phosphogypsum (HPG) and calcium carbide slag (CS), were selected to activate wet ground granulated blast furnace slag (WGGBS) and three different phosphate tailings backfill materials were prepared. Fluidity, rheology, settling ratio, compressive strength, water resistance and ion leaching behavior of backfill materials were determined. According to the results, when either PG or HPG is used as the sole activator, the fluidity properties of the materials are enhanced. Phosphate tailings backfill material activated with PG present the largest fluidity and the lowest yield stress. Furthermore, the backfill material's compressive strength is considerably increased to 2.9 MPa at 28 days after WGGBS activation using a mix of HPG and CS, all with a settling ratio of only 1.15 percent. Additionally, all the three ratios of binder have obvious solidification effects on heavy metal ions Cu and Zn, and P in phosphate tailings.

KEYWORDS

Fluidity; rheology; compressive strength; phosphate tailing; backfill material

1 Introduction

With the increasing demand for mineral resources for social development, the excessive discharge of tailings has caused serious safety problems [1]. In order to solve the structural instability of mining areas caused by the overexploitation of minerals and the resulting surface storage of tailings, cemented tailings backfill (CTB) has become the most promising method of mining backfill [2–5]. This is due to its excellent mechanical properties and simpler process [6].

However, CTB uses cement as the binder material, which presents a challenge in achieving optimal fluidity and cost-effectiveness. The utilization of industrial solid wastes for the preparation of low-cost binders and their application to backfill material is of interest to a wide range of researchers [7]. As research continues, the significance of the cooperative production of backfill material from a wide range



of solid wastes is becoming increasingly evident as a pivotal instrument in the green transformation of the mining industry [8]. In particular, in the area of clinker-free backfill material, researchers have conducted numerous studies on the use of tailings as fine aggregates. Wang et al. [9] prepared cementitious materials based on limestone tailings using desulfurized gypsum, slag, cement clinker, and sodium hydroxide. They also investigated the effects of fineness modulus, cement-sand ratio, and slurry concentration on the flow and strength of the cementitious materials. Zhang et al. [10] used 0.075~0.6 mm copper tailings sand as a substitute for natural fine aggregates. Then they used copper tailings powder, slag and fly ash to prepare geopolymer paste composites. The results showed that the optimal replacement rate of copper tailings sand was 20%, and the total replacement rate of copper tailings in geopolymer mortar could be up to 33%.

In order to mitigate the environmental impact of tailings storage and optimize the utilization of solid waste, the use of total solid waste as backfill material has been demonstrated to be a viable approach. Lv et al. [11] proposed a magnesium coal-based backfill material with modified magnesium slag and fly ash as a binder, coal gasification coarse slag and coal gangue as an aggregate which has a 28-days compressive strength that reached a maximum of 10.21 MPa. He et al. [12] produced clinker-free cemented iron tailings backfill material with 28 days compressive strength of 3.7 MPa. The above studies can be summarized to show that the main concerns at present are how to optimize the design of the mixing ratio to increase the activation efficiency of solid wastes, and how to refine solid wastes and add activators to improve the strength of the backfill material.

Among the many studies on the preparation of cementitious materials from industrial solid wastes, the synergistic replacement of cement with refined granulated blast-furnace slag, the hemihydrate phosphogypsum (HPG), and carbide slag (CS), which are three representative types of industrial solid wastes, has been shown to have good applicability and prospects [13]. The wet milling process refines the ground granulated blast-furnace slag (GGBS) and mechanically activates it. Furthermore, the HPG and CS stimulate the GGBS. Additionally, phosphate tailings (PT), as a potential secondary mineral resource, can be comprehensively recycled to recover useful elements such as Ca and Mg, and a series of high value-added materials can be prepared [14].

On the basis of previous studies, this study extended the process of wet milling treatment for GGBS with different ratios of binder systems (HPG-activated/phosphogypsum-activated/HPG-CS synergistic excitation) and added PT as fine aggregate to form three kinds of clinker-free cementitious backfill material based on phosphate tailings. In this paper, the fluidity, rheological properties, compressive strength, settling ratio, water resistance, porosity, and ion-leaching behavior of the three backfill materials were investigated. The aim is to further investigate the effect of the ratio of clinker-free cementitious materials on phosphate tailings backfill material.

2 Experimental





2.1 Materials

PT used in this study was supplied by Hubei Xingfa Chemicals Group Co., Ltd., Yichang, China. CS with a median particle size of 34.4 μm ($418.6 \text{ m}^2/\text{kg}$) was obtained from Hubei Yihua Group Co., Ltd., Yichang, China. Dihydrate phosphogypsum (PG) is a kind of industrial byproduct gypsum produced during the production of high-concentration phosphorus fertilizer, with a median particle size of 44.1 μm ($320.1 \text{ m}^2/\text{kg}$), from Hubei Yihua Group Co. (China). HPG was produced by burning of PG at a temperature of approximately 200°C. HPG was obtained from Wuhan Iron and Steel (Group) Co., Wuhan, China. GGBS was provided by Wuhan Iron and Steel (Group) Company Limited. The raw slag was dry milled to become powdery and white in color. The chemical compositions and contents of the five raw materials are shown in [Table 1](#). Pictures of the raw materials are shown in [Table 2](#).

Table 1: Chemical composition of the raw materials

Type	Oxide compositions (wt.%)							
	SiO ₂	CaO	Al ₂ O ₃	MgO	SO ₃	P ₂ O ₅	Fe ₂ O ₃	LOI
PT	7.36	27.72	12.71	13.09	0.79	5.28	0.59	32.46
CS	2.3	63.7	1.6	0.1	0.3	0	0.1	31.9
PG	6.0	32.3	0.4	0.1	46.8	1.2	0.3	12.9
HPG	5.7	38.3	0.5	0	48.8	2.0	0.6	4.1
GGBS	36.9	38.6	12.3	7.4	2.1	0	0.3	2.4

Table 2: Images of the raw materials

Raw material	Images	State
PT		Particle
CS		Powder
PG		Powder
HPG		Powder
GGBS		Powder

2.2 Preparation of Specimens

A vertical ball mill was used to prepare wet ground granulated blast-furnace slag (WGGBS) [15]. The mass ratio of grinding balls to GGBS powder to water was 16:6:3. After mixing, it was poured into a grinding equipment and ground at 400 rpm/min for 40 min to obtain WGGBS slurry with a median particle size of 1.19 μm (by laser diffraction particle size analyzer). The three backfill materials were designed according

to the ratio in Table 3. Samples were prepared and cured under standard conditions for 7 days before demolding. At 7, 28 and 56 days, the compressive strength of the specimens of backfill material was tested.

Table 3: The ratio of three backfill materials

Number	WGGBS (%)	HPG (%)	PG (%)	CS (%)	Binder-tailing ratio	Slurry concentration (%)
WP-1	80	15	0	5	1:12	76
WP-2	80	20	0	0	1:12	76
WP-3	80	0	20	0	1:12	76

Note: Sample number is WP-1, where W denotes WGGBS and P denotes phosphate tailings as fine aggregate. Slurry concentration is the mass of the clinker-free binder and phosphate tailings divided by the total mass.

2.3 Testing Methods

2.3.1 Fluidity

The height of the round mold used for the fluidity test is 150 mm, the inner diameter of the upper opening is 50 mm, the inner diameter of the lower opening is 100 mm, and the inner wall is smooth and without seams in the metal products. The pounding rod should be a steel rod with a diameter of 8 mm and a length of 300 mm, and the end should be rounded off. Flatten the surface after a total of 30 ramming strokes. After the surface was thoroughly leveled, the mold was lifted upwards at a steady speed. After about 10 s, measure the maximum length in the line segments that are perpendicular to each other in both directions.

2.3.2 Rheological Properties

The RST touch screen rheometer from BROOKFIELD was used. The instrument parameters were a torque of 100 mN·m, torque resolution of 0.15 $\mu\text{N}\cdot\text{m}$, and a rate range of 0.01–1200 RPM. The slurry was tested in two modes of constant shear rate/non-constant shear stress, and the constant shear rate mode was used to shear the slurry at a rate of 100 s^{-1} for 8 min and then stop the operation.

2.3.3 Compressive Strength

A fully automatic compression testing machine (DYE-300A) was used to test the compressive strength at a loading rate of 2.4 kN/s. The mortar was poured into the iron mold (40 mm \times 40 mm \times 40 mm). The specimens were placed in a standard curing room and cured until they reached the required age. The average of three tests was taken as the final compressive strength value.

2.3.4 Settling Ratio

The well-mixed backfill slurry was loaded into a measuring cup with a total volume of 1000 mL up to the 500 mL mark, weighed as m_1 shaken well and left to settle naturally, and weighed as m_2 after 28 days of placing it under standard curing conditions. At 25°C and standard atmospheric pressure, the density of water was 0.99705 g/cm^3 , or ρ_1 . This is how the settling ratio (S) was computed [16]:

$$S = \frac{(m_1 - m_2)/\rho_1}{500} \quad (1)$$

2.3.5 Water Resistance

The mixed fresh slurry mixture was poured into a steel mold (40 mm \times 40 mm \times 40 mm) and placed on a mortar vibration table for vibrating and compacting. The molds were placed in a standard curing room (ambient temperature 20°C \pm 2°C, relative humidity 95% \pm 2%) and cured until hardened before demolding. The specimens were demolded and then cured for 28 days, and then dried in an oven at 100°C \pm 5°C until the mass of the specimens was completely stable, and the specimens' compressive strength was evaluated. F is the material's compressive strength while it is dry, and f is the material's

compressive strength when it is saturated with water. The softening coefficient (K) is a parameter that indicates the property of water resistance, the value of K ranges from 0 to 1, the larger the value, the better the water resistance of the material, and its expression is as follows:

$$K = \frac{f}{F} \quad (2)$$

2.3.6 Porosity

The specimens were demolded and then kept in water for 27 days under standard curing conditions. After the completion of water retention, the specimens were removed and the excess water was wiped off. The mass of the specimens was weighed as M_1 . Next, the specimens were baked in an oven at $100^\circ\text{C} \pm 5^\circ\text{C}$ for 24 h until the mass of the specimens was totally stable, and the mass of the specimens was weighed as M_2 . Porosity was calculated using the formula:

$$\alpha = \frac{M_1 - M_2}{M_2} \quad (3)$$

2.3.7 SEM

A scanning electron microscope (FE-SEM, QUAN-TAFEG 450) was used to study the microscopic structure of the clinker-free binder. The acceleration voltage of the instrument was adjusted from 0.3 to 30 kV. The test blocks were removed after the drying treatment and cut into 2–3 mm diameter to be used for testing. To obtain clearer images, gold plating was used to ensure good electrical conductivity of the specimens.

2.3.8 Ion-Leaching Behavior

A plasma emission spectrometer manufactured by Leman-Lebers Company, USA, was used to measure the ion-leaching behavior. The instrumental test parameters were: wavelength range of 165–1100 nm, continuous wavelength coverage, optical resolution of 0.007 nm, and analytical accuracy of less than 2%.

3 Results and Discussion

3.1 Fluidity Analysis

The ability of the backfill slurry to flow through the pipeline is an important indicator of its pumpability [17]. A low water-cement ratio increases material cost and results in dry, viscous backfill material with decreased fluidity. It is important to analyze the fluidity of the backfill material. In this paper, the fluidity of backfill material is studied under three different mixing ratios, and the results are shown in Fig. 1.

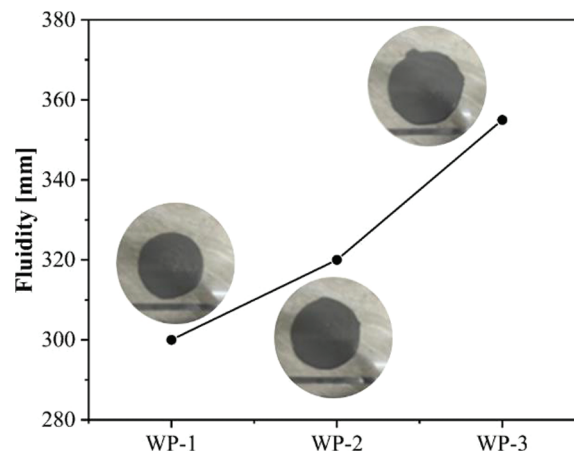


Figure 1: Fluidity of three backfill materials

The results are shown in Fig. 1. It can be seen that backfill material with three different mixing ratios has great fluidity (>220 mm) when the slurry consistency is fixed at 76% and the gray-to-sand ratio is fixed at 1:12. The fluidity of WP-1, WP-2, and WP-3 was increased to 300, 320, and 355 mm, respectively. Compared to WP-1, WP-2 showed a 6.7% increase in mobility. It is easy to find that WP-3 with the addition of PG has higher fluidity than WP-2. This is because the specific surface area of PG is larger than that of HPG and CS [13]. In conclusion, either PG, HPG or HPG composite CS activates WGGBS to form a binder that can effectively inhibit precipitation, improve the continuity of the backfill slurry, and improve the fluidity, and also improve the pipeline transportation performance of the backfill slurry to a certain extent.

3.2 Rheological Properties Analysis

Rheological properties describe the deformation and fluidity of a material under the shear action of external forces. They also allow for quantitative analysis of the stress and strain relationship of the material at a certain moment by establishing a series of rheological models [18]. Most cementitious composite systems exhibit non-Newtonian fluid characteristics. The Bingham model, Modified-Bingham model, and Herschel-Bulkley model are commonly used to quantify the key parameters of rheological properties. In this subsection, the H-B model is used to match the rheological profile of the backfill material and investigate its properties [19,20]. The model's rheological equation is:

$$\tau = \tau_0 + K\dot{\gamma}^n \quad (4)$$

τ is the shear stress in Pa, τ_0 is the yield stress in Pa; K is the coefficient of consistency in $(\text{Pa}\cdot\text{s}^n)$; n is the Fluidity index; $\dot{\gamma}$ is the shear rate in $1/\text{s}$.

The impact of shear stress (a) and yield stress (b) of backfill materials with different mixing ratios is shown in Fig. 2. The shear stress of the three types of backfill materials showed a non-linear relationship with the shear rate. At a certain shear rate, the shear stresses of WP-1, WP-2, and WP-3 decreased sequentially. Additionally, the yield stresses of WP-1, WP-2, and WP-3 also decreased gradually, which is consistent with the pattern of the fluidity. This may be determined by the difference in the early hydration rates of them. Further analysis of the specific effects of the three different mixing ratios of activators on the hydration of WGGBS will be made in the chapter on compressive strength. As can be seen from Table 4, the fluidity index of WP-1, WP-2 and WP-3 gradually increased, which can satisfy the needs for the filling slurry pipelines' self-flowing transportation.

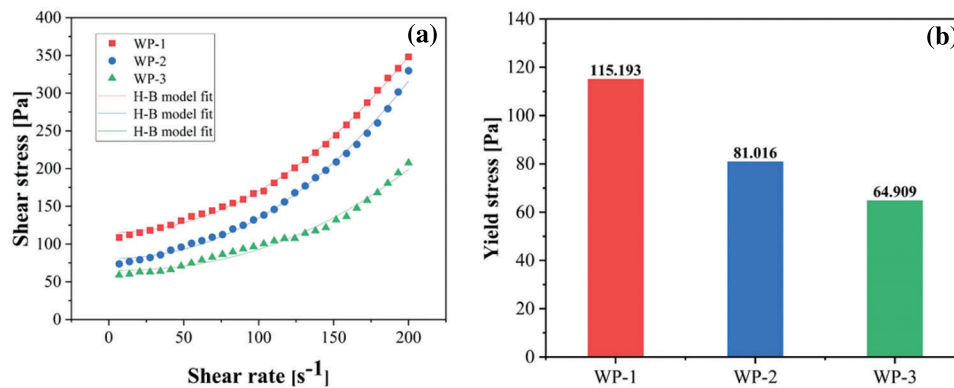


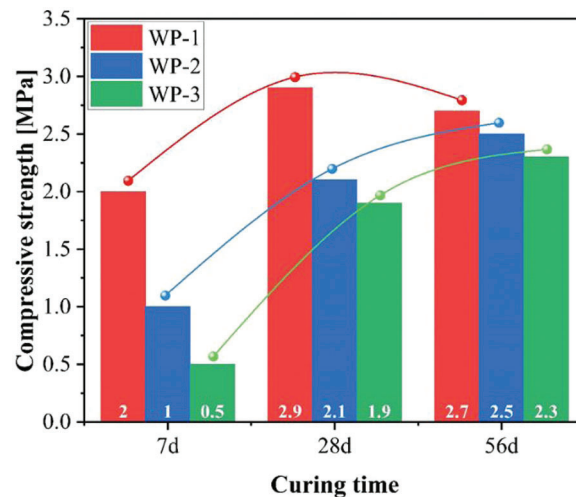
Figure 2: Shear stress (a) and yield stress (b) of three backfill materials

Table 4: H-B model fitting of rheological parameters of backfill materials

Sample	Fitted equation	Yield stress τ_0 (Pa)	Consistency coefficient (Pa·s ⁿ)	Fluidity index	Correlative coefficient
WP-1-1	$\tau = 115.193 + 0.0038\gamma^{2.082}$	115.193	0.0038	2.082	0.998
WP-1-2	$\tau = 81.016 + 0.0023\gamma^{2.138}$	81.016	0.0023	2.138	0.996
WP-1-3	$\tau = 64.909 + 0.0019\gamma^{2.257}$	64.909	0.0019	2.257	0.985

3.3 Compressive Strength Analysis

The compressive strength of three different backfill materials mixing ratios at various curing periods is shown in Fig. 3. It should be noted that the strengths of the three backfill materials at 3 days were not considered due to their inability to be removed from the mold at 3 days. This is mainly caused by the lower reactivity of GGBS in the cementitious material compared to ordinary cement and the lower gray-to-sand ratio. The three backfill materials have the same strength regularity at different curing times. WP-1 has the highest strength, followed by WP-2, and WP-3 has the lowest strength. The strength of WP-3 also reached 1.9 MPa after 28 days of curing, which fully satisfied the limiting strength requirement of backfill material (0.5 MPa). The strength of the material depends on the activity of WGGBS, which has been confirmed in previous studies [13]. In comparison to WP-3, the HPG used in WP-2 is more reactive than PG and generates PG more rapidly upon contact with water [12]. The newly generated PG is highly reactive and can produce calcium aluminosilicate hydrate (C-A-S-H) and ettringite (AFt) when combined with WGGBS. These compounds act as fillers, further increasing the strength [21]. In contrast, PG has low solubility in WP-3, resulting in the production of relatively little AFt during the reaction with WGGBS. In WP-1, $\text{Ca}(\text{OH})_2$ in CS provides a favorable alkaline environment for the hydration of GGBS, which accelerates its hydration [22]. The excitation effect of HPG also contributes to this process. The combined excitation of the two resulted in the generation of a more network-like C-A-S-H and AFt inside the material, forming a dense structure that enhanced the sample's strength [23].

**Figure 3:** Compressive strength of three backfill materials at different curing times

During the curing process from 7 to 56 days, the compressive strength of WP-1 increased significantly compared to WP-2 and WP-3. At 7 days, the compressive strength of WP-1 was 2 MPa, whereas the compressive strengths of WP-2 and WP-3 were 1 and 0.5 MPa, respectively, which increased by 100%

and 300% compared to WP-2 and WP-3, respectively. Both increase rates decreased as curing time increased, indicating that the composite excitation effect of HPG and CS on WGGBS is most pronounced in the early stages. It is possible that the early increase in rate is due to a decrease in phosphorus content [24]. Further analysis on this point will be conducted in the chapter on ion-leaching behavior.

The compressive strengths of the other groups exhibited a gradual increasing trend with the age of curing, except for WP-1, which showed a decrease in strength at a later stage. This suggests that the HPG and CS-inspired WGGBS systems may lead to an unstable long-term strength of the filler materials. The strength reduction may be attributed to the expansion of the specimens and the concentration of internal stresses caused by excessive AFt crystals generated at a later stage [23]. However, the material still maintained a high compressive strength of 2.7 MPa, which was higher than that of WP-2 and WP-3 (2.5 and 2.3 MPa). In conclusion, for the three different ratios of solid waste binder, both HPG and PG contribute sufficiently to meet the strength requirements. Compared to using only HPG or PG to excite WGGBS, the composite excitation of WGGBS with HPG and CS can significantly improve the compressive strength of the backfill material. This leads to more complete hydration of WGGBS and has a beneficial effect on the early strength growth of the material. Therefore, it can be concluded that the use of CS-gypsum composite excitation with WGGBS provides a greater advantage in terms of compressive strength.

3.4 Settling Ratio Analysis

The settling refers to the change in the volume of material during backfilling. The settling ratio of backfill material is affected by a number of factors, such as the backfilling method, the type of material, etc., and drying shrinkage due to evaporation of water is one of the most important factors [25].

As shown in Fig. 4, the settling ratio of three backfill materials at 28 days for different ratios was compared. At 28 days, WP-1 has the best settling properties with a settling ratio of 1.15%, which is lower than 4.23% and 4.78% for WP-2 and WP-3, respectively. WP-1 meets the settling ratio requirement of S1 grade of Tailings Sand Concrete for Mining Blanket Filling (JC/T 2478-2018), whereas WP-2 and WP-3 satisfied the S2 grade requirement of JC/T 2478-2018 [26]. Combined with the strength analysis in the previous chapter, it can be seen that the WGGBS in WP-1 has the most complete reaction. Generally, higher gel content leads to higher strength and a lower settling ratio. The settling ratio of WP-2 was decreased by 11.5% compared to that of WP-3. Analogous to the reason for the difference in compressive strength, it is primarily attributed to the high reactivity of HPG itself, which quickly generates PG upon contact with water. The newly generated PG reacts with the WGGBS to produce AFt in the pore space, acting as a backbone for support and stability that prevents settling.

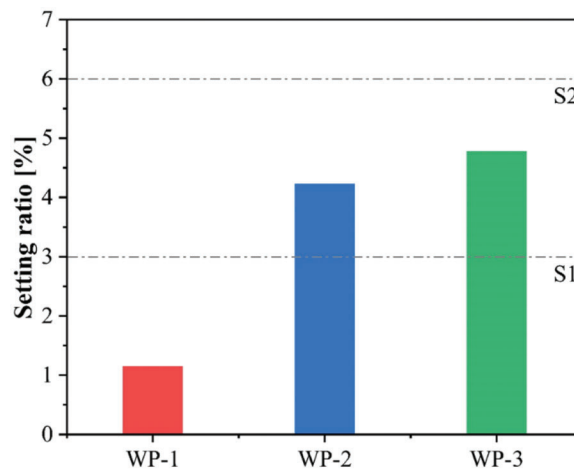


Figure 4: Settling ratio of three backfill materials

3.5 Water Resistance and Porosity Analysis

The softening coefficient is suitable for expressing the water resistance of backfill material [27]. In this study, the softening coefficients of three backfill materials at 28 days were compared (Fig. 5) to provide a reference for the durability of three mixing ratios of backfill material in water-bearing environments. Porosity in Fig. 6 was measured using the water saturation method instead of traditional mercury intrusion porosimetry. This method is more accurate in measuring unconnected pores and micropores and is also more convenient and time-saving.

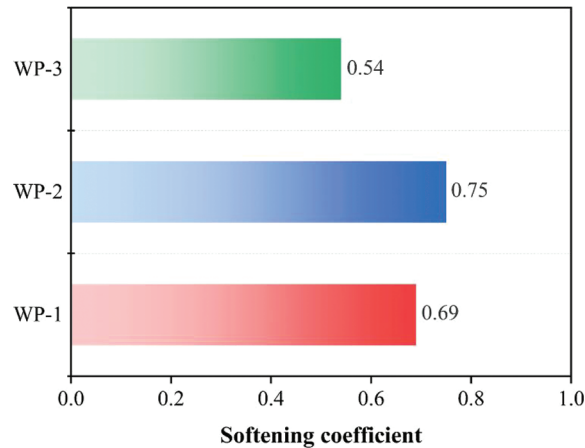


Figure 5: Softening coefficients of three backfill materials

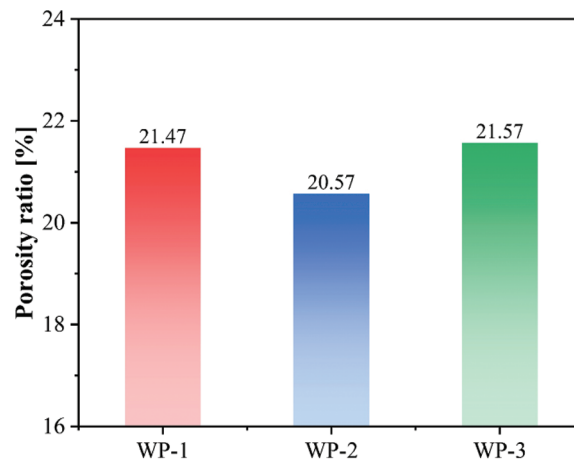


Figure 6: Porosity of three backfill materials

As can be seen in Fig. 5, the softening coefficients of WP-1, WP-2, and WP-3 are 0.69, 0.75, and 0.54, respectively, and the porosity is 21.47%, 20.57%, and 21.57%, respectively. Among them, WP-2 has the highest softening coefficients and the lowest porosity. Compared with WP-3, the softening coefficients of WP-1 increased by 38.9% and the porosity decreased. The trend of porosity of different samples in Fig. 6 is consistent with the trend of water resistance in Fig. 5. It is easy to understand that the improvement of water resistance is mainly affected by porosity, and the abundant C-A-S-H gels in WP-2 can be connected with each other to form a mesh to make the structure denser, which is the fundamental reason

for the good water resistance of the material. It can also be found that the softening coefficients of WP-1 decreased by 8% and porosity increased by 4.4% compared to that of WP-2. This is related to the factors for the decline in strength of WP-1 at 56 d in Section 3.3. Specifically, the specimen swelled due to the excess AFt crystals in WP-1, loosening the structure, which increased water absorption, increased porosity, and decreased the specimen's water resistance.

3.6 SEM Analysis

Fig. 7 displays the morphology of the hydration products of WP-1 and WP-2, which exhibit a significant variability in their hydration products. The specific hydration products, namely C-A-S-H and AFt, have been labeled in the figure. WP-1 contains a large amount of C-A-S-H gel and short columnar AFt can also be observed as shown in Fig. 7a. The co-existence of gel and AFt in WP-1 is attributed to the synergistic excitation of HPG and CS. The intertwining of AFt with C-A-S-H gel results in a denser pore structure. In Fig. 7b, WP-2 exhibits a sparser structure due to the fact that its hydration products are predominantly long and coarse AFt. This indicates that the products without CS are coarser AFt and less gel content.

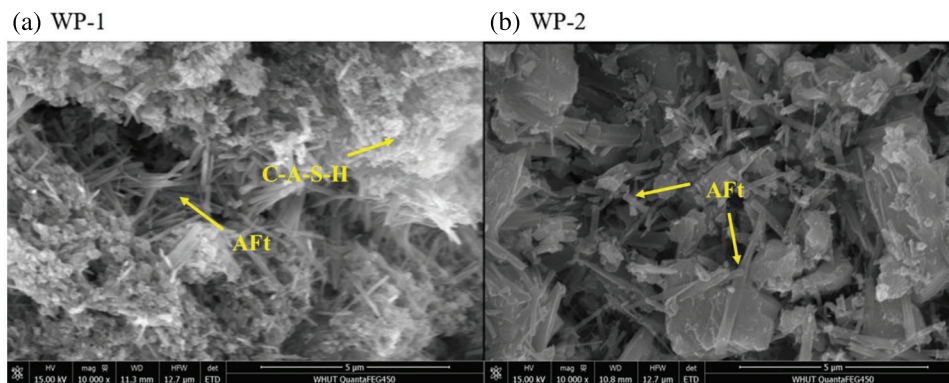


Figure 7: SEM images of paste on 28 days

3.7 Ion-Leaching Behavior Analysis

During the backfilling process, the leaching of phosphorus (P) and heavy metal ions in PT will bring great harm to the environment. In particular, the dissolution of P may lead to eutrophication of lakes and rivers, which in turn causes imbalance in the local ecosystem [28]. Based on the consideration of environmental sustainability, it is essential to observe the exudation of elemental P and other heavy metal ions when backfilling the PT.

As shown in Fig. 8, the ion-leaching behavior of the original PT and the three backfill materials cured for 28 days was compared. As can be seen from Fig. 8a, the Ca ions leaching from the original PT were the largest, reaching 487.234 ppm. The leaching of harmful P ions also reached 3.1523 ppm. Meanwhile, the heavy metal ions Cu and Zn, which pollute the environment, were partially leached. Compared to the original PT, the leaching of Mg and Si ions in WP-1, WP-2, and WP-3 was significantly reduced. The leaching of Ca ions was significantly reduced to 94.648, 96.422, and 96.491 ppm, respectively. This reduction was mainly due to the consumption of Ca ions by the generation of gels [29]. These results demonstrate that the three types of clinker-free cementitious backfill materials based on phosphate tailings exhibit good consolidation and compressive strength. WP-1 exhibited the greatest reduction in Ca ions, which further confirms the conclusion that the HPG and CS composites have the most effective activation of GGBS.

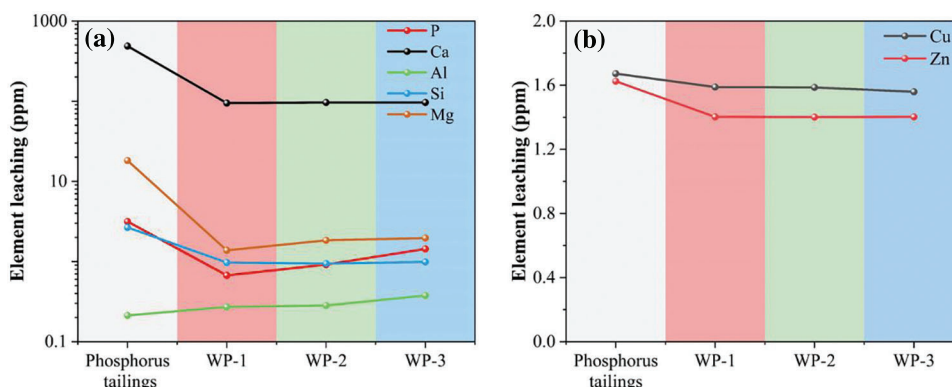


Figure 8: Ion-leaching behavior of three backfill materials

It is noteworthy that among the four specimens, WP-1 has the least leaching of P ions, which may be related to the fact that the three cementitious materials have the least amount of PG doping. In addition, the leaching of P ions decreased sequentially in the order of WP-1, WP-2, and WP-3, which was consistent with the performance of the pattern of early strength. Since it was mentioned in the chapter on compressive strength analysis that the lower P content may be one of the reasons for the excellent early strength performance of WP-1, this fact of P ions leaching provides a basis for this inference. First, the presence of acidic soluble P, soluble F, and other impurities in PT and PG is detrimental to HPG hydration [30,31]. The $[\text{PO}_4]^{3-}$ ions in the liquid phase limited the generation of AFt, while the $[\text{SO}_4]^{2-}$ ions inhibited the hydration of C_3A . For the WP-2 system, the retardation effect of P is mainly in the form of PO_4^{3-} adsorption on the HPG surface, which can delay the early hydration of HPG to some extent [32]. For the WP-3 system, the soluble P_2O_5 in PT and PG exists in the form of H_3PO_4 in water, which lowers the pH of the pore solution in the slurry, which is unfavorable to the formation of $\text{Ca}(\text{OH})_2$ and C-A-S-H, and thus affects the early strength of the backfill material. Due to the presence of CS in the WP-1 system, $\text{Ca}(\text{OH})_2$ in CS can react with H_3PO_4 in a neutralization reaction to produce $\text{Ca}_3(\text{PO}_4)_2$ precipitation, which simultaneously releases the activity of HPG and WGGBS. As shown in Fig. 8b, the leaching of Cu ions and Zn ions from the three backfill materials also decreased compared to the original PT. It shows that the cementitious material has a good solidifying effect on the tailings and can reduce the harm of heavy metal ions to the environment.

4 Conclusion

In the present study, a certain amount of HPG, PG, and a composite of HPG and CS were used to activate the WGGBS respectively, and three different clinker-free cementitious backfill materials based on phosphate tailings were prepared.

(1) When either PG or HPG is used as the sole activator, both are able to improve the fluidity properties of the materials. Phosphate tailings backfill material activated with PG has the highest fluidity and the lowest yield stress.

(2) WP-1 showed the best settling properties due to the inhibition of sedimentation of the combined HPG and CS-activated WGGBS, with a settling ratio of 1.15%. This was 72.5% and 75.9% lower compared to 4.23% and 4.78% for WP-2 and WP-3 at 28 days, respectively.

(3) The use of HPG as an activator is more effective in enhancing the compressive strength of phosphate tailings backfill material. Based on this, a certain proportion of CS can maximize the strength of the backfill material, reaching 2 MPa at 7 days and 2.9 MPa at 28 days. SEM analysis shows that the synergistic excitation of HPG and CS led to the generation of reticular C-A-S-H and AFt in WP-1, forming a dense

gel structure. However, excessive AFt generation may cause back shrinkage of strength, but the compressive strength of WP-1 still reached an acceptable 2.7 MPa at 56 days.

(4) Phosphate tailings backfill with HPG as the activator results in a denser pore structure compared to using only PG as the activator. This leads to better water resistance.

(5) All three ratios of binder have a significant solidifying effect on heavy metal ions such as Cu and Zn, as well as P in PT. Reducing the leaching of Cu and Zn ions can reduce the hazards to the surrounding environment due to the backfilling of PT. Reducing the leaching of P can minimize its negative impact on early strength.

The three backfill materials in this study meet the basic performance requirements of the mining area. However, their economic benefits have not been quantitatively analyzed. Future studies should combine economic and environmental analyses with the actual situation to evaluate their economic and ecological benefits.

Acknowledgement: The authors express their gratitude to the editors and reviewers for their insightful comments that helped to raise the caliber of our manuscript.

Funding Statement: The authors would like to acknowledge the Key Research and Development Program of Hubei Province (2022BCA071) and the Wuhan Science and Technology Bureau (2022020801020269).

Author Contributions: The authors confirm contribution to the paper as follows: study conception and design: Jin Yang, Senye Liu; data collection: Xingyang He, Senye Liu; analysis and interpretation of results: Ying Su, Jin Yang, Jingyi Zeng, Senye Liu; draft manuscript preparation: Bohumír Strnadel, Jin Yang, Senye Liu. All authors reviewed the results and approved the final version of the manuscript.

Availability of Data and Materials: The data used to support the findings of this study are available from the corresponding author upon request.

Conflicts of Interest: The authors declare that they have no conflicts of interest to report regarding the present study.

References

1. Zhao Y, Zhang Y, Chen T, Chen Y, Bao S. Preparation of high strength autoclaved bricks from hematite tailings. *Constr Build Mater.* 2012;28(1):450–5. doi:10.1016/j.conbuildmat.2011.08.078.
2. Kasap T, Yilmaz E, Sari M. Physico-chemical and micro-structural behavior of cemented mine backfill: effect of pH in dam tailings. *J Environ Manage.* 2022;314:115034. doi:10.1016/j.jenvman.2022.115034.
3. Behera SK, Ghosh CN, Mishra K. Utilisation of lead-zinc mill tailings and slag as paste backfill materials. *Environ Earth Sci.* 2020;79:1–18.
4. Deng XJ, Liu H, Zhang JX, Zhao YL, Li Y, Bian LG et al. Study on microbial cemented backfill mining technology. *J Min Sci Technol.* 2023;8(4):439–51.
5. Li JL, Li A, Hao JZ, Xu JY, Zhang LB. Experimental study on the ratio between ti-bearing blast furnace slag-iron-based full tailing sand and cement in cementitious filling. *J Min Sci Technol.* 2023;8(6):838–46.
6. Zhang X, Wu D, Lu H, Liu L, Zheng S. Improvement of tailings gradation on workability and strength of cemented tailings backfill. *Constr Build Mater.* 2023;387:131633. doi:10.1016/j.conbuildmat.2023.131633.
7. Edraki M, Baumgartl T, Manlapig E, Bradshaw D, Franks DM, Moran C. Designing mine tailings for better environmental, social and economic outcomes: a review of alternative approaches. *J Clean Prod.* 2014;84:411–20. doi:10.1016/j.jclepro.2014.04.079.
8. Zheng Y, Xiao J, Cheng J. Industrial structure adjustment and regional green development from the perspective of mineral resource security. *Int J Environ Res Pub Health.* 2020;17(19):6978. doi:10.3390/ijerph17196978.

9. Wang Y, Li Z, Jin Q, Zhang M, Zhou Z. High-efficiency utilization of limestone tailings: used as cementitious materials and fine aggregate to prepare karst structure filling material. *Constr Build Mater.* 2022;316:125841. doi:10.1016/j.conbuildmat.2021.125841.
10. Zhang Y, Liu H, Ma T, Chen CL, Gu GH, Wang JH, et al. Experimental assessment of utilizing copper tailings as alkali-activated materials and fine aggregates to prepare geopolymer composite. *Constr Build Mater.* 2023;408:133751. doi:10.1016/j.conbuildmat.2023.133751.
11. Lv Y, Liu L, Yang P, Xie G, Zhang C, Deng S. Study on leaching and curing mechanism of heavy metals in magnesium coal based backfill materials. *Process Saf Environ.* 2023;177:1393–402. doi:10.1016/j.psep.2023.07.084.
12. He XY, Li WL, Yang J, Su Y, Zhang YN, Zheng JY, et al. Multi-solid waste collaborative production of clinker-free cemented iron tailings backfill material with ultra-low binder-tailing ratio. *Constr Build Mater.* 2023;367:130271. doi:10.1016/j.conbuildmat.2022.130271.
13. Yang J, Zeng JY, He XY, Zhang YN, Su Y, Tan HB. Sustainable clinker-free solid waste binder produced from wet-ground granulated blast-furnace slag, phosphogypsum and carbide slag. *Constr Build Mater.* 2022;330:127218. doi:10.1016/j.conbuildmat.2022.127218.
14. Moukannaa S, Loutou M, Benzaazoua M, Vitola L, Alami J, Hakkou R. Recycling of phosphate mine tailings for the production of geopolymers. *J Clean Prod.* 2018;185:891–903. doi:10.1016/j.jclepro.2018.03.094.
15. Liu Q, Chen S, He XY, Su Y, Zeng JY, Zhu Y, et al. Surface modification of fly ash by waste engine oil under mechanical activation enhanced the sustainable service life of asphalt. *J Clean Prod.* 2023;404:136785. doi:10.1016/j.jclepro.2023.136785.
16. Angle CW, Gharib S. Effects of sand and flocculation on dewaterability of kaolin slurries aimed at treating mature oil sands tailings. *Chem Eng Res Des.* 2017;125:306–18. doi:10.1016/j.cherd.2017.07.014.
17. Roshani A, Fall M. Rheological properties of cemented paste backfill with nano-silica: link to curing temperature. *Cement Concrete Comp.* 2020;114:103785. doi:10.1016/j.cemconcomp.2020.103785.
18. Barnes HA. The yield stress—A review or ‘*παντα ρει*’—everything flows? *J Non-Newton Fluid.* 1999;81(1–2):133–78.
19. Wang ZB, Fan YR, Zuo JP. The impact of temperature and pre-wetting of aggregates on rheological properties of coal gangue mortars. *J Min Sci Technol.* 2024;9(2):190–8.
20. Nguyen VH, Remond S, Gallias JL. Influence of cement grouts composition on the rheological behaviour. *Cement Concrete Res.* 2011;41(3):292–300. doi:10.1016/j.cemconres.2010.11.015.
21. Gijbels K, Lacobescu RI, Pontikes Y, Schreurs S, Schroevers W. Alkali-activated binders based on ground granulated blast furnace slag and phosphogypsum. *Constr Build Mater.* 2019;215:371–80. doi:10.1016/j.conbuildmat.2019.04.194.
22. Fernández-Jiménez A, Vázquez T, Palomo A. Effect of sodium silicate on calcium aluminate cement hydration in highly alkaline media: a microstructural characterization. *J Am Ceram Soc.* 2011;94(4):1297–303. doi:10.1111/jace.2011.94.issue-4.
23. Li L, Shi Z, Ai Y. Alkaline activation of gypsum-granulated blast furnace slag cementing materials. *J Chin Ceram Soc.* 2008;36(3):405–10.
24. Wang L, Luo RY, Zhang W, Jin MM, Tang SW. Effects of fineness and content of phosphorus slag on cement hydration, permeability, pore structure and fractal dimension of concrete. *Fractals.* 2021;29(2):2140004. doi:10.1142/S0218348X21400041.
25. Sadeghian G, Behfarnia K, Teymouri M. Drying shrinkage of one-part alkali-activated slag concrete. *J Build Eng.* 2022;51:104263. doi:10.1016/j.jobe.2022.104263.
26. Chu CF, Deng YF, Zhou AN, Feng Q, Ye H, Zha FS. Backfilling performance of mixtures of dredged river sediment and iron tailing slag stabilized by calcium carbide slag in mine goaf. *Constr Build Mater.* 2018;189:849–56. doi:10.1016/j.conbuildmat.2018.09.049.
27. Khalil AA, Tawfik A, Hegazy AA. Plaster composites modified morphology with enhanced compressive strength and water resistance characteristics. *Constr Build Mater.* 2018;167:55–64. doi:10.1016/j.conbuildmat.2018.01.165.

28. Huang S, Voutchkov N, Jiang S. Balancing carbon, nitrogen and phosphorus concentration in seawater as a strategy to prevent accelerated membrane biofouling. *Water Res.* 2019;165:114978. doi:10.1016/j.watres.2019.114978.
29. Daher S, Benazzouk A, Hamed HB, Langlet T. Performance improved of a lime and hemp-based concrete through the addition of metakaolin. *Fluid Dyn Mater Proc.* 2023;19(5):1091–113. doi:10.32604/fdmp.2023.020348.
30. Kaziliunas A, Leskeviciene V, Vektaris B, Valancius Z. The study of neutralization of the dihydrate phosphogypsum impurities. *Ceram-Silikaty.* 2006;50(3):178.
31. Singh M. Role of phosphogypsum impurities on strength and microstructure of selenite plaster. *Constr Build Mater.* 2005;19(6):480–6. doi:10.1016/j.conbuildmat.2004.07.010.
32. Jiang GZ, Wu AX, Wang YM, Li JQ. Effect of lime on properties of filling cementitious material prepared by hemihydrate phosphogypsum. *J Chin Ceram Soc.* 2020;48:86–93.